Supporting Information

Grueter et al. 10.1073/pnas.1221742110

SI Methods

Viral-Mediated Gene Transfer. For cell type–specific expression and behavioral assays, we used herpes simplex viral (HSV) vectors encoding GFP under control of the CMV promoter without (HSV-GFP) or with (HSV-LS1-ΔFosB) ΔFosB following a stop codon surrounded by loxP sites driven by the IE 4/5 promoter allowing expression of GFP in all transduced cells and expression of ΔFosB only in cells also expressing Cre recombinase. Published HSV vectors were used in other experiments (1). Expression of the HSV transgene is maximal between 1 and 4 d after infusion and dissipates completely by day 7 (2). Therefore, behavioral assays began 24 h after stereotaxic introduction of the viral vectors.

Stereotaxic Surgery. Adult mice (male, D1-Cre or D2-Cre, 15–30 g) were used. Mice were anesthetized with a mixture of ketamine (100 mg/kg) and xylazine (10 mg/kg) and positioned in a small animal stereotaxic instrument. Nucleus accumbens (NAc) was targeted bilaterally using the following stereotaxic coordinates: + 1.6 (anterior/posterior), +1.5 (lateral), and −4.4 (dorsal/ventral) at an angle of 10° from the midline (relative to Bregma). The core and shell subregions of NAc are affected equally by these injections (the two subregions cannot reliably be targeted selectively in a mouse). A total of 0.5 μL of purified virus was delivered on each side over a 4-min period, followed by 6 min of rest. In all behavioral experiments, proper NAc targeting of virus infusion was confirmed post hoc by preparing brain slices and visual confirmation of both needle track and GFP expression by confocal microscopy. For electrophysiology and morphology experiments, data were collected from GFP-positive cells and adjacent GFP-negative cells as controls.

Cocaine Place Preference and Locomotor Responses. The place conditioning procedure was conducted as previously described (1). Briefly, 2 d before intra-NAc infusions of HSV-GFP or HSV-LS1-DFosB into D1-Cre or D2-Cre mice, animals were placed into the conditioning chambers, which consist of three contextually distinct environments. Mice displaying significant preference for either of the two conditioning chambers were excluded from the study (<10% of all animals). Conditioning groups were further balanced to adjust for any chamber bias that still may exist. Two days after surgery, animals were injected with saline and confined to one chamber in the morning for 30 min and then injected with cocaine (3.75 or 7.5 mg/kg, i.p.) and confined for 30 min to the other chamber in the afternoon for 2 consecutive d, equaling a total of two rounds of association training per treatment (two saline and two cocaine pairings). On the day of the test, mice were placed back into the apparatus without treatment for 20 min and tested to evaluate side preference. Locomotor responses to cocaine were assessed via beam breaks in the cocaine-paired chambers for the 2 treatment d and then again with a third injection just after the preference test on the third day, for a total of three locomotor measurements. For all groups, baseline locomotion in response to saline was assessed to determine the effects of genotype and viral transgene expression on baseline locomotor activity.

Electrophysiology. Parasagittal slices (250 μm) containing the NAc were prepared from D1-tdTomato heterozygous bacterial artificial chromosome (BAC) transgenic mice on a C57BL/6j background (8–10 wk of age) as described previously (3, 4), 3–4 d after HSV-ΔFosB-EGFP infection. Briefly, following euthanasia under isoflurane, brains were quickly removed and placed in an ice-cold low sodium/high sucrose dissecting solution. Slices were cut by adhering the two sagittal hemispheres of brain containing the NAc to the stage of a Leica vibroslicer. Slices were allowed to recover for a minimum of 60 min in a submerged holding chamber (~25 °C) containing artificial cerebrospinal fluid (ACSF) consisting of (in mM) 124 NaCl, 4.4 KCl, 2.5 $CaCl_2$, 1.3 $MgSO_4$, 1 NaH_2PO_4, 11 glucose, and 26 $NaHCO_3$. Slices were then removed from the holding chamber and placed in the recording chamber where they were continuously perfused with oxygenated (95% O_2/5% CO_2) ACSF at a rate of 2 mL/min at 30 ± 2 °C. Picrotoxin (50 μM) was added to the ACSF to block $GABA_A$ receptor–mediated inhibitory synaptic currents.

Whole-cell voltage-clamp recordings from medium spiny neurons (MSNs) were obtained using infrared differential interference contrast (IR-DIC) video microscopy. NAc shell and core subregions were identified by the presence or absence of anterior commisure and stria present dorsal to the NAc. D1-tdTomato and ΔFosB expressing MSNs in the NAc were identified by the presence of EGFP and tdTomato that were excited with UV light using bandpass filters (HQ470/40× and HQ545/×30 exciter filter, respectively). We define D2 MSNs as those MSNs lacking tdTomato, a conclusion validated in previous studies (3). Recordings were made with electrodes (3.0–6.0 MΩ) filled with (in mM) 120 $CsMeSO_4$, 15 CsCl, 8 NaCl, 10 Hepes, 0.2 EGTA, 10 TEA-Cl, 4 Mg^{2+}ATP, 0.3 Na^{2+}GTP, 0.1 spermine, and 5 QX-314. Excitatory afferents were stimulated with a bipolar nichrome wire electrode placed within the NAc, roughly 100 μm dorsal and rostral to the recorded cell. Recordings were performed using a Multiclamp 700B (Molecular Devices), filtered at 2 kHz, and digitized at 10 kHz. Excitatory postsynaptic currents (EPSCs) of 100–400 pA were evoked at a frequency of 0.1 Hz while MSNs were voltage-clamped at –70 mV unless otherwise stated. Data acquisition and analysis were performed on-line using custom Igor Pro software. Input resistance and access resistance were monitored continuously throughout the duration of each experiment, which was terminated if these changed by >20%. Paired-pulse ratios (PPRs) were acquired by applying a second afferent stimulus of equal intensity at a specified time after the first stimulus and then calculating EPSC1/EPSC2. For a given interstimulus interval for each cell, the PPRs of six responses were averaged. AMPA receptor (AMPAR)/NMDA receptor (NMDAR) ratios were calculated as the ratio of the magnitude of the peak amplitude of the EPSCs recorded at –70 mV (AMPAR EPSCs) and at +40 mV at 50 ms following afferent stimulation (NMDAR EPSCs). Miniature EPSCs were collected at a holding potential of –70 mV in the presence of 500 nM TTX. Ten-second blocks of events were acquired and analyzed using Minianalysis software (Synaptosoft) with threshold parameters set at 6-pA amplitude and <3-ms rise time. All events included in the final data analysis were verified by eye. The CV was calculated as the SD of the AMPAR and NMDAR EPSC amplitudes divided by the mean for epochs of 30 consecutive trials. Our analysis was based on $1/CV^2$ (5, 6). AMPAR current-voltage relationship analysis was done in the presence of 100 μM APV. The rectification index is reported as the ratio of the peak current at –40 mV/peak current at +40 mV in the presence of 100 μM APV.

Data Analysis. Values are expressed as mean ± SEM (n = number of cells for electrophysiology; number of dendrites for morphology; and number of animals for behavior). Two-tailed Student's test was used for statistical analysis, and $P < 0.05$ was considered statistically significant.

Drugs. The following drugs were purchased from Sigma-Aldrich: cocaine HCl, picrotoxin, and TTX. The following reagents were purchased from Tocris: D-(-)-2-Amino-5-phosphonopentanoic acid (D-APV) and 2,3-Dioxo-6-nitro-1,2,3,4-tetrahydrobenzo[*f*] quinoxaline-7-sulfonamide (NBQX).

1. Maze I, et al. (2010) Essential role of the histone methyltransferase G9a in cocaine-induced plasticity. *Science* 327(5962):213–216.
2. Barrot M, et al. (2002) CREB activity in the nucleus accumbens shell controls gating of behavioral responses to emotional stimuli. *Proc Natl Acad Sci USA* 99(17): 11435–11440.
3. Grueter BA, Brasnjo G, Malenka RC (2010) Postsynaptic TRPV1 triggers cell type-specific long-term depression in the nucleus accumbens. *Nat Neurosci* 13(12):1519–1525.
4. Grueter BA, et al. (2006) Extracellular-signal regulated kinase 1-dependent metabotropic glutamate receptor 5-induced long-term depression in the bed nucleus of the stria terminalis is disrupted by cocaine administration. *J Neurosci* 26(12):3210–3219.
5. Marie H, Morishita W, Yu X, Calakos N, Malenka RC (2005) Generation of silent synapses by acute in vivo expression of CaMKIV and CREB. *Neuron* 45(5):741–752.
6. Kullmann DM (1994) Amplitude fluctuations of dual-component EPSCs in hippocampal pyramidal cells: implications for long-term potentiation. *Neuron* 12(5):1111–1120.

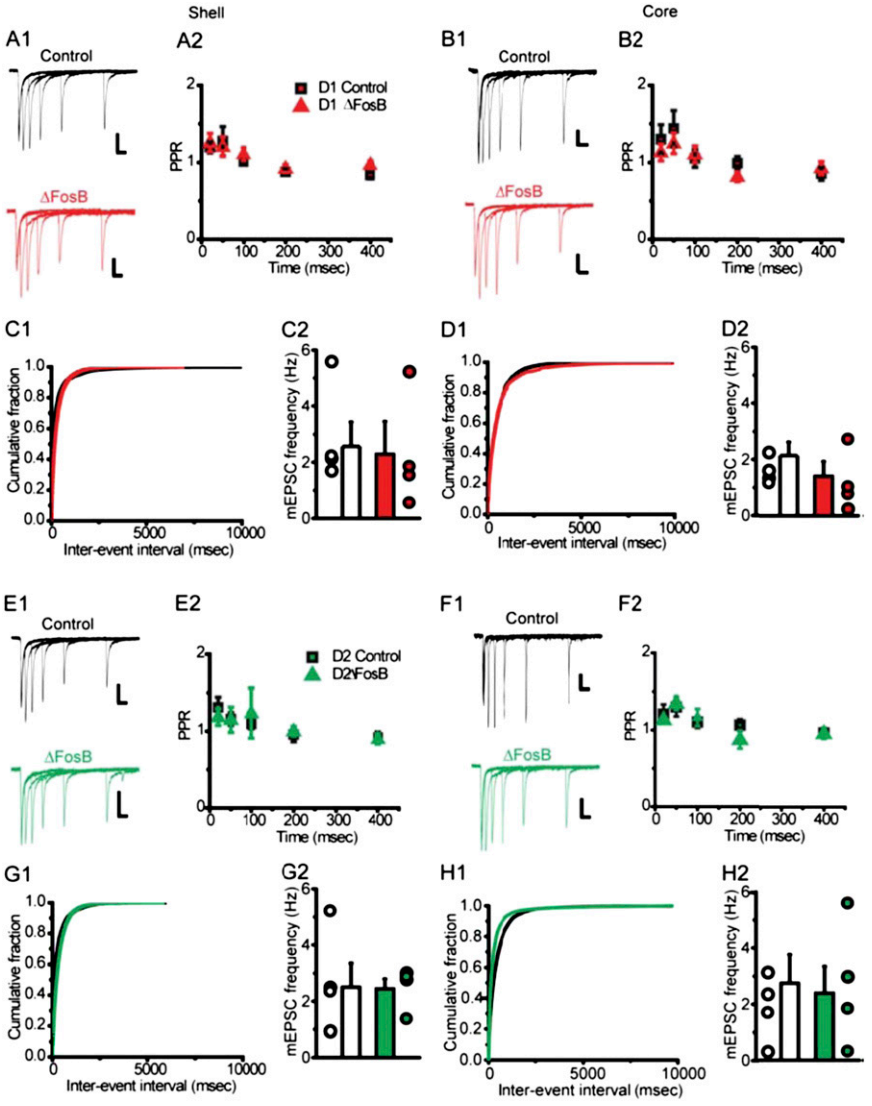

Fig. S1. Presynaptic properties of D1 and D2 MSNs in the NAc shell overexpressing ΔFosB. (*A1*) Sample traces from NAc shell of D1 ΔFosB(–) and D1 ΔFosB(+) EPSCs at 20-, 50-, 100-, 200-, and 400-ms interstimulus intervals. (*A2*) Summary graph of PPRs from D1 ΔFosB(–) (open symbols; $n = 7$) and D1 ΔFosB(+) (filled symbols; $n = 7$) MSNs (calibration bars for evoked EPSCs in this panel and all subsequent figures unless noted are 50 pA/25 ms). (*B1*) Sample traces from NAc core of D1 ΔFosB(–) and D1 ΔFosB(+) EPSCs at 20-, 50-, 100-, 200-, and 400-ms interstimulus intervals. (*B2*) Summary graph of PPRs from NAc core D1 ΔFosB(–) and D1(+) ΔFosB(+) MSNs ($n = 6$–7). (*C1*) Cumulative probability plot of mEPSC frequencies recorded from D1 ΔFosB(–) and D1 ΔFosB(+) MSNs. (*C2*) Summary graph of mean ± SEM for NAc shell D1 ΔFosB(–) and D1 ΔFosB(+) MSNs ($n = 5$–6). (*D1*) Cumulative probability plot of mEPSC frequencies recorded from NAc core D1 ΔFosB(–) and D1 ΔFosB(+) MSNs. (*D2*) Summary graph of mEPSC frequency mean ± SEM for the two populations of NAc core D1 ΔFosB(–) and D1 ΔFosB(+) MSNs ($n = 4$ each). (*E1*) Sample traces from NAc shell of D2 ΔFosB(–) and D2 ΔFosB(+) EPSCs at 20-, 50-, 100-, 200-, and 400-ms interstimulus intervals. (*E2*) Summary graph of PPRs from D2 ΔFosB(–) (filled squares; $n = 6$) and D2 ΔFosB(+) (triangles; $n = 6$) MSNs. (*F1*) Sample traces from NAc core of D2 ΔFosB(–) and D2 ΔFosB(+) EPSCs at 20-, 50-, 100-, 200-, and 400-ms interstimulus intervals. (*F2*) Summary graph of PPR from NAc core D2 ΔFosB(–) and D2 ΔFosB(+) MSNs ($n = 6$–7). (*G1*) Cumulative probability plot of mEPSC frequencies recorded from D2 ΔFosB(–) and D2 ΔFosB(+) MSNs. (*G2*) Summary graph of mEPSC frequency mean ± SEM for NAc shell D2 ΔFosB(–) and D2 ΔFosB(+) MSNs ($n = 5$–6). (*H1*) Cumulative probability plot of mEPSC frequencies recorded from NAc core D2 ΔFosB(–) and D2 ΔFosB(+) MSNs. (*H2*) Summary graph of mEPSC frequency mean ± SEM for the two populations of NAc core D2 ΔFosB(–) and D2 ΔFosB(+) ($n = 4$ each).

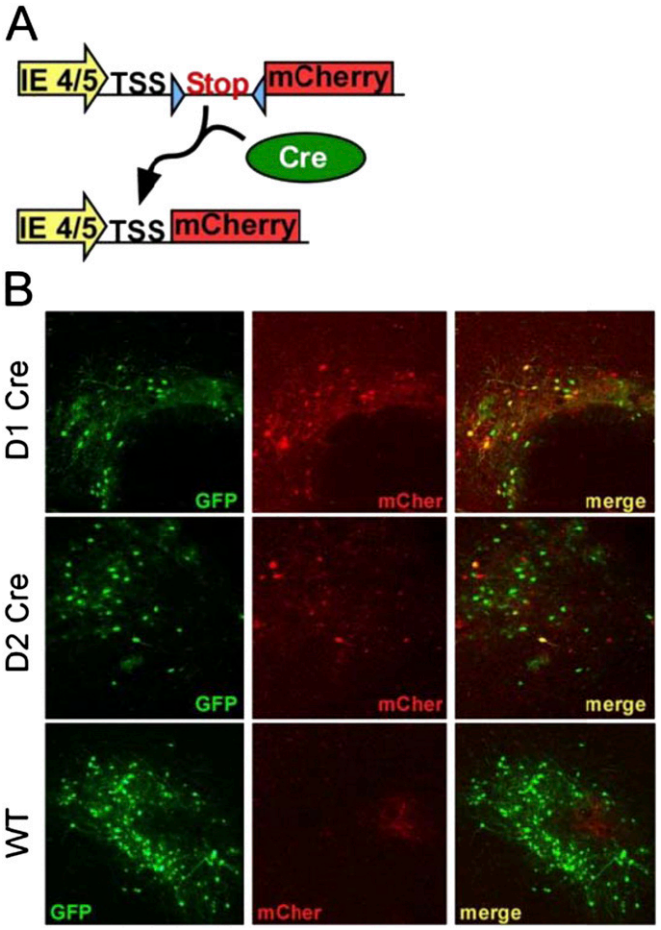

Fig. S2. Identification of D1 and D2 MSNs for spine quantification. (*A*) Design of Cre-dependent mCherry HSV expression vector (HSV-LS1-mCherry). A stop codon surrounded by loxP sites (blue triangles) is excised by Cre recombinase to allow expression of the target gene, mCherry. (*B*) Mouse NAc was injected with HSV-LS1-mCherry and either GFP-FosB or GFP alone. mCherry is expressed selectively in D1- and D2-Cre mice, but is not expressed in WT littermates. GFP fluorescence was used to quantify spines in cells that were also mCherry positive in D1-Cre or D2-Cre mice (Fig. S3).

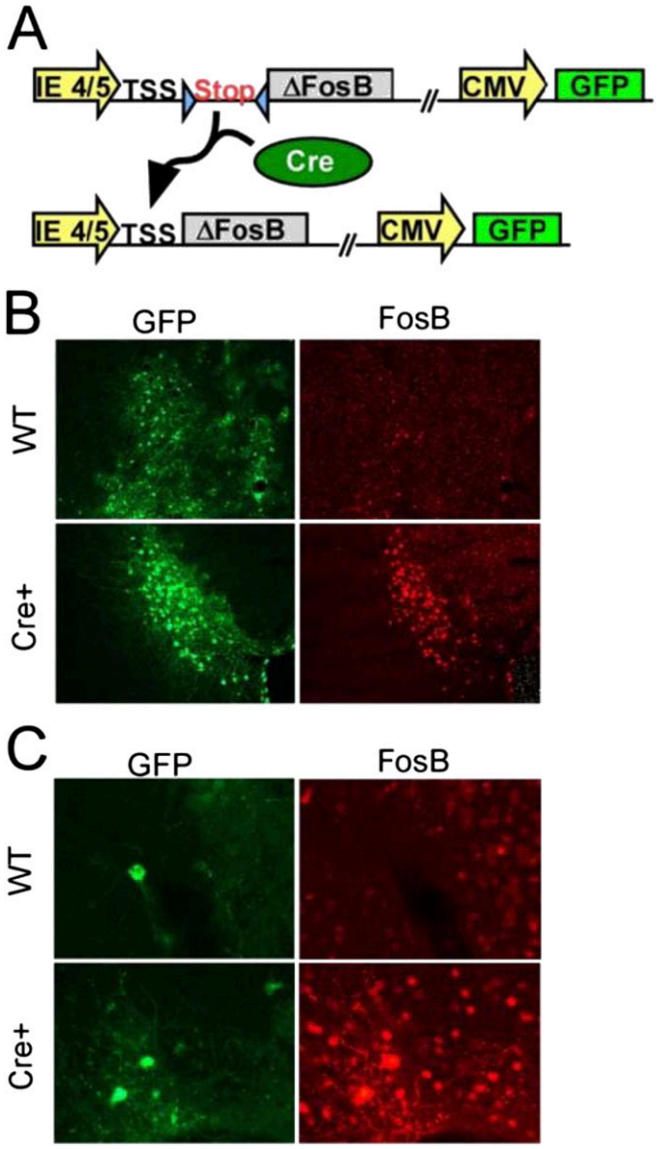

Fig. S3. Strategy for short-term cell type–specific overexpression of ΔFosB for behavioral assays. (*A*) HSV vector design depicting loxP-surrounded stop codon between IE 4/5 promoter–driven transcriptional start site and sequence encoding ΔFosB, followed by constitutive CMV promoter–driven GFP. Cells expressing Cre recombinase (green) remove the stop sequence, allowing IE 4/5 to drive production of FosB. (*B*) 10× and (*C*) 40× immunohistochemical images of GFP (green) expression in all transduced cells, and FosB (red) expression in Cre-expressing animals (Cre+) but not WT littermates (WT).